PERGAMON

Mechanism and Machine Theory 36 (2001) 1189–1202

MECHANISM AND MACHINE THEORY

www.elsevier.com/locate/mechmt

Mathematical model and undercutting of cylindrical gears with curvilinear shaped teeth

Rui-Tang Tseng, Chung-Biau Tsay *

Department of Mechanical Engineering, National Chiao Tung University, 1001, TA Hseuh Road, Hsinchu 30010, Taiwan, ROC

Received 10 July 2000; received in revised form 12 July 2001; accepted 28 July 2001

Abstract

A rack cutter with a curved-tooth is considered the generating tool for the generation of the proposed gear, and a mathematical model of cylindrical gears with curvilinear shaped teeth is developed according to the gearing theory. The developed computer program can develop profiles of the curvilinear-tooth gear with point contacts. The developed gear tooth mathematical model is used to investigate the tooth undercutting of curvilinear-tooth gears via differential geometry and the numerical method.

1. Introduction

Gear manufacturers and designers continuously attempt to develop more compact and higher capacity gear pairs. A positive-shifted gear or a gear with a larger pressure angle has a larger tooth root-thickness, which can increase the root strength of the gear. Moreover, gear pairs with higher contact ratios can reduce the tooth contact and bending stresses.

Liu [1] discussed the characteristics of curvilinear-tooth gears and proposed manufacturing cylindrical gears with curvilinear shaped teeth. That investigation applied a face mill-cutter to generate curvilinear-tooth gears and suggested the merits of curvilinear-tooth gears which are as follows: higher bending strengths, lower noise, better lubrication conditions, and no axial thrust forces. Dai et al. [2] investigated manufacturing a cylindrical gear with curved teeth via a computer numerically controlled (CNC) hobbing machine with male and female flying cutters. Although they analyzed the fundamental characteristics of the gears based on the experimental

* Corresponding author. Tel.: +886-35-728-450; fax: +886-35-728-450.
E-mail address: cbtsay@cc.nctu.edu.tw (C.-B. Tsay).

0094-114X/01/$ - see front matter
PII: S0094-114X(01)00049-0

Nomenclature

$a_F,\ b_F$	tool setting of rack cutter Σ_F (Fig. 3)
l_F	variable parameter which determines the location on rack cutter (Fig. 3)
$[M_{ca}]$	coordinate transformation matrix; transforming from coordinate system S_a to coordinate system S_c
M_n	normal module (Fig. 3)
$\mathbf{N}_c^{(F)}$	normal vector of surface Σ_F represented in coordinate system S_c
$\mathbf{n}_c^{(F)}$	unit normal vector of surface Σ_F represented in coordinate system
$\mathbf{R}_a^{(i)}$	position vector of surface i $(i = F, 1)$ represented in coordinate system S_a
R_F	nominal radius of the face mill-cutter (Fig. 4)
r_1	radius of pitch circle of gear 1
$S_i^{(F)}(X_i^{(F)}, Y_i^{(F)}, Z_i^{(F)})$	coordinate system i $(i = a, c)$ with three mutual perpendicular axes $X_i^{(F)}$, $Y_i^{(F)}$ and $Z_i^{(F)}$ (Fig. 4)
$S_i(X_i, Y_i, Z_i)$	coordinate system i $(i = 1, h)$ with three mutual perpendicular axes X_i, Y_i and Z_i (Fig. 5)
W	face width (Fig. 4)
θ_F	variable parameter which determines the location on rack cutter (Fig. 4)
θ_{Fu}	the upper bound of parameter θ_F
θ_{Fl}	the lower bound of parameter θ_F
ρ_F	fillet radius of rack cutter Σ_F (Fig. 3)
Σ_F	generating rack cutter surface F
Σ_1	generated tooth surface 1
ϕ_1	rotation angle of gear 1 when gear 1 is generated by rack cutter Σ_F (Fig. 5)
$\psi_n^{(F)}$	normal pressure angel of rack cutter Σ_F (Fig. 3)
Subscripts	
F	generating rack cutter surface
1	generated tooth surface

method, their proposed gear pairs are in line contact and the transmission errors of these gear pairs are sensitive to gear axial misalignments.

The gear and pinion with curvilinear shaped teeth proposed herein are generated by the same cutter, and the tooth mathematical model of curvilinear-tooth gears is developed according to the gearing theory. The rack cutter with a curved-tooth is considered the generating tool for the generation of the proposed gear. Three-dimensional tooth surfaces of curvilinear-tooth gears can be plotted by applying the computer graphics. The proposed curvilinear-tooth gear is not sensitive to gear axial misalignments since the bearing contact of the gear pair is located on the middle region of the gear tooth surfaces. It is due to the fact that the curvatures of the mating tooth surfaces are different. One of the mating tooth surfaces is cut by inside face mill-cutter and the other mating tooth surface is cut by outside face mill-cutter which has different nominal radii of face mill-cutter, as shown in Fig. 1. The curvilinear-tooth gear pair proposed in [1] is in line contact. However, the curvilinear-tooth gear pair proposed in our paper is in point contact. Therefore, the main advantage of the proposed gear pair is not sensitive to gear axial misalign-

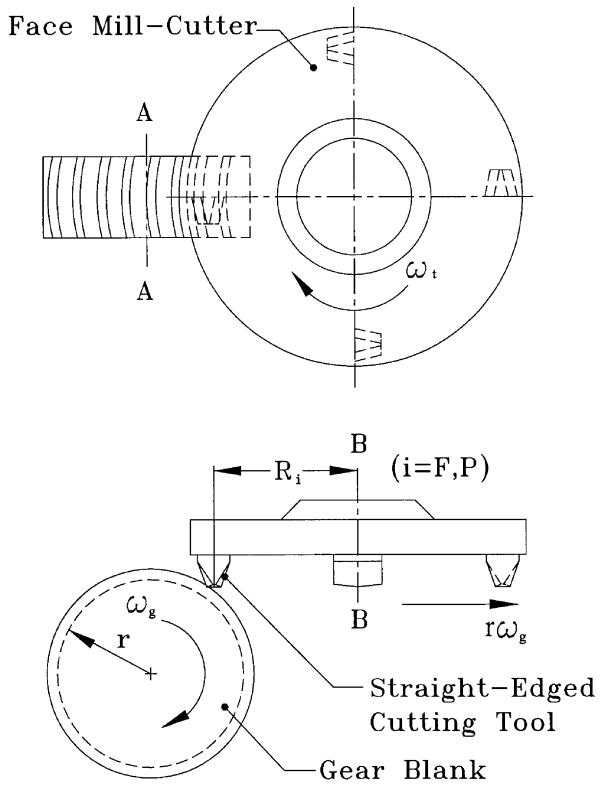

Fig. 1. Generating mechanism for curvilinear-tooth gears.

ments. Besides, only one cutter is needed for our cutting of the proposed type of gearing, while the generation method proposed in [1] needs two different cutters. However, compared with the line contact gearing, the load capacity of point contact gearing is relatively small, and this is the main disadvantage of the proposed gear. However, by properly choosing the nominal radius of the face mill-cutter, the contact ellipses can be enlarged and the load capacity can thus be increased.

As is well known, gears with tooth undercutting may decrease the gear strength. Kin [3] applied the contact-line envelope and the pressure-angle limit concepts to prevent the tooth undercutting of worm and worm gear surfaces. Fong and Tsay [4] utilized surface unit normal vectors to investigate the tooth undercutting of spiral bevel gears, while Litvin [5,6] provided a detailed investigation of the singularity and tooth undercutting. This study also analyzes the tooth undercutting of curvilinear-tooth gears according to the developed gear mathematical model and the gearing theory.

2. A mathematical model of cylindrical gears with curvilinear shaped teeth

Fig. 1 illustrates the generating mechanism for cylindrical gears with curvilinear shaped teeth [1], where axis *A–A* represents the rotation axis of the gear blank, axis *B–B* expresses the cutter

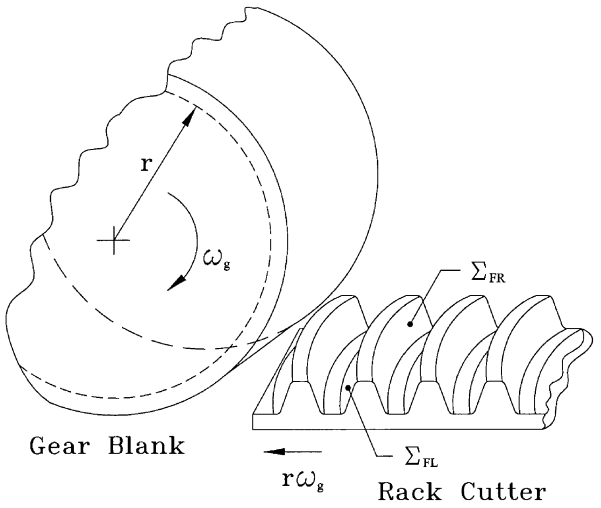

Fig. 2. Relations between the rack cutter and gear blank.

spindle, R_i denotes the nominal radius of the face mill-cutter, and r indicates the radius of the gear pitch circle. During the generation process, the cutter spindle moves rightward with velocity $r\omega_g$ and rotates clockwise with angular velocity ω_t while the gear blank rotates clockwise with angular velocity ω_g. This generating process will produce one space and the gear blank is indexed to one tooth and the generating cycle is repeated until all the teeth and spaces are produced.

The manufacturing of cylindrical gears with curvilinear shaped teeth can be simulated by considering the meshing of a gear blank with a rack cutter as depicted in Fig. 2. During the generation process, the rack cutter translates with velocity $r\omega_g$ while the gear blank rotates with angular velocity ω_g, where r represents the radius of the gear pitch circle. The tooth form of rack cutter in the longitudinal direction is a circular arc tooth rather than a straight tooth that generates the spur gears.

2.1. Normal middle section of the rack cutter

Fig. 3 depicts the normal middle section of the rack cutter $\Sigma_F^{(n)}$ that generates the gear space. The profile of the rack cutter's normal middle section is the same as the straight-edged rack cutter that generates the tooth profile of involute gears. The normal middle section of rack cutter $\Sigma_F^{(n)}$ consists of two parts: the straight line $\overline{M_0^{(F)}M_2^{(F)}}$ and the circular arc of radius ρ_F with its center at C_F as displayed in Fig. 3. The straight line generates the working part of the gear tooth surface while the circular arc produces the fillet surface. Parameters a_F, b_F, M_n, $\psi_n^{(F)}$, l_F and ρ_F are the design parameters of the normal middle section of the rack cutter $\Sigma_F^{(n)}$. Fig. 3 reveals that both sides of the rack cutter normal middle section are symmetrical. The straight line $\overline{M_0^{(F)}M_2^{(F)}}$ of the normal middle section of the rack cutter can be represented in the coordinate system $S_a^{(F)}(X_a^{(F)}, Y_a^{(F)}, Z_a^{(F)})$ by

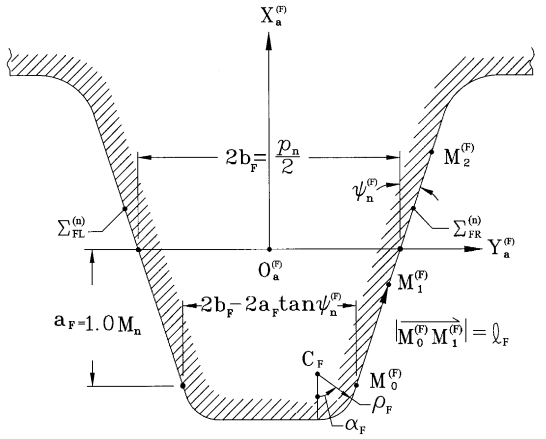

Fig. 3. Normal middle section of rack cutter $\Sigma_F^{(n)}$.

$$\mathbf{R}_a^{(F)} = \begin{bmatrix} l_F \cos\psi_n^{(F)} - a_F \\ \pm(l_F \sin\psi_n^{(F)} + b_F - a_F \tan\psi_n^{(F)}) \\ 0 \end{bmatrix}, \tag{1}$$

where the design parameters, a_F and b_F, can determine the coordinates of the initial point, $M_0^{(F)}$, of the straight line $\overline{M_0^{(F)} M_2^{(F)}}$. l_F represents the distance measured from the initial point $M_0^{(F)}$, moving along the straight line $\overline{M_0^{(F)} M_2^{(F)}}$, to any point $M_1^{(F)}$ on the right-side normal middle section of the rack cutter $\Sigma_{FR}^{(n)}$. Point $M_0^{(F)}$ of the normal middle section of the rack cutter $\Sigma_{FR}^{(n)}$ generates the lowest point of the working part of the tooth surface Σ_{1L}. The upper sign in Eq. (1) represents the right-side of the normal middle section of the rack cutter $\Sigma_{FR}^{(n)}$ while the lower sign depicts the left-side of the normal middle section of the rack cutter $\Sigma_{FL}^{(n)}$.

2.2. Rack cutter surfaces

The mathematical model of the right- and left-side rack cutter surfaces should be individually expressed since the right- and left-side surfaces of the rack cutter are not symmetrical as illustrated in Fig. 2. The right-side of the rack cutter surface Σ_{FR} is used to generate the left-side of the curvilinear gear tooth surface Σ_{1L}, while the left-side of the rack cutter surface Σ_{FL} is used to produce the right-side of the curvilinear gear tooth surface Σ_{1R}.

Fig. 4 depicts the formation of the rack cutter surface and the relations between coordinate systems $S_a^{(F)}(X_a^{(F)}, Y_a^{(F)}, Z_a^{(F)})$ and $S_c^{(F)}(X_c^{(F)}, Y_c^{(F)}, Z_c^{(F)})$. The rack cutter surface Σ_F is formed in the coordinate system $S_c^{(F)}$ as the normal middle section of the rack cutter $\Sigma_F^{(n)}$, represented in the coordinate system $S_a^{(F)}$, moves along the circular-arc $\widehat{AB}$. Circular-arc $\widehat{AB}$ stands for the tooth traces of the rack cutter, $C_t^{(F)}$ denotes the center of the circular-arc $\widehat{AB}$, W designates the width of the rack cutter (also the face width of the gears), and R_F denotes the radius of the circular-arc $\widehat{AB}$ (the nominal radius of the face mill-cutter as illustrated in Fig. 1). The homogeneous coordinate transformation from coordinate system $S_a^{(F)}$ to coordinate system $S_c^{(F)}$ can be represented as

$$\mathbf{R}_c^{(F)} = [M_{ca}]\mathbf{R}_a^{(F)}, \tag{2}$$

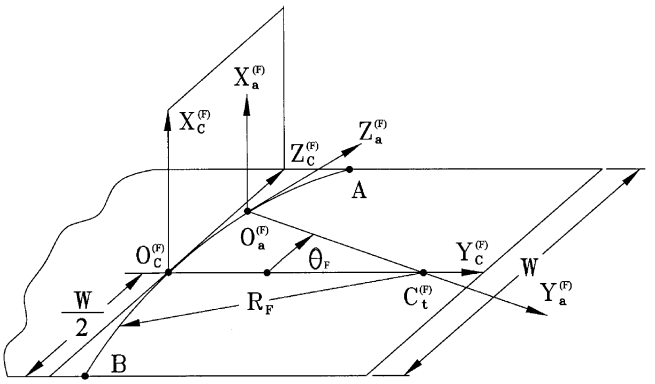

Fig. 4. Relations between coordinate systems $S_c^{(i)}$ and $S_a^{(i)}$.

where

$$[M_{ca}] = \begin{bmatrix} 1 & 0 & 0 & 0 \\ 0 & \cos\theta_F & \sin\theta_F & R_F(1-\cos\theta_F) \\ 0 & -\sin\theta_F & \cos\theta_F & R_F\sin\theta_F \\ 0 & 0 & 0 & 1 \end{bmatrix}.$$

Substituting Eq. (1) into Eq. (2) yields the equation of the rack cutter surface Σ_F represented in coordinate system $S_c^{(F)}$ as

$$\mathbf{R}_c^{(F)} = \begin{bmatrix} l_F\cos\psi_n^{(F)} - a_F \\ \pm(l_F\sin\psi_n^{(F)} + b_F - a_F\tan\psi_n^{(F)})\cos\theta_F + R_F(1-\cos\theta_F) \\ \mp(l_F\sin\psi_n^{(F)} + b_F - a_F\tan\psi_n^{(F)})\sin\theta_F + R_F\sin\theta_F \end{bmatrix}, \tag{3}$$

where

$$\theta_{Fl} \leqslant \theta_F \leqslant \theta_{Fu}, \quad \theta_{Fl} = \sin^{-1}\left(\frac{-W}{2R_F}\right), \quad \theta_{Fu} = \sin^{-1}\left(\frac{-W}{2R_F}\right) \tag{4}$$

and R_F is the radius of the curve $\overset{\frown}{AB}$. Parameter θ_F is the surface parameter of the rack cutter surface as determined by Eq. (4).

The normal vector $\mathbf{N}_c^{(F)}$ and unit normal vector $\mathbf{n}_c^{(F)}$ of the rack cutter surface Σ_F can be obtained and represented in coordinate system $S_c^{(F)}$ as

$$\mathbf{N}_c^{(F)} = \frac{\partial\mathbf{R}_c^{(F)}}{\partial l_F} \times \frac{\partial\mathbf{R}_c^{(F)}}{\partial\theta_F} \tag{5}$$

and

$$\mathbf{n}_c^{(F)} = \frac{\mathbf{N}_c^{(F)}}{\left|\mathbf{N}_c^{(F)}\right|}, \tag{6}$$

where the position vector $\mathbf{R}_c^{(F)}$ denotes the equation of the rack cutter surface Σ_F represented in coordinate system $S_c^{(F)}$. Symbols l_F and θ_F are the surface coordinates of the rack cutter surface. According to Eqs. (3), (5) and (6), the unit normal vector of the rack cutter surface Σ_F is

$$\mathbf{n}_{\mathrm{c}}^{(\mathrm{F})} = \begin{bmatrix} \pm \sin\psi_{\mathrm{n}}^{(\mathrm{F})} \\ -\cos\psi_{\mathrm{n}}^{(\mathrm{F})}\cos\theta_{\mathrm{F}} \\ \cos\psi_{\mathrm{n}}^{(\mathrm{F})}\sin\theta_{\mathrm{F}} \end{bmatrix}. \tag{7}$$

The upper sign in Eqs. (3) and (7) represents the right-side of the rack cutter surface Σ_{FR} while the lower sign denotes the left-side of the rack cutter surface Σ_{FL}.

2.3. Equation of meshing

Fig. 5 displays the schematic relationship among coordinate systems $S_{\mathrm{c}}^{(\mathrm{F})}(X_{\mathrm{c}}^{(\mathrm{F})}, Y_{\mathrm{c}}^{(\mathrm{F})}, Z_{\mathrm{c}}^{(\mathrm{F})})$, $S_1(X_1, Y_1, Z_1)$ and $S_{\mathrm{h}}(X_{\mathrm{h}}, Y_{\mathrm{h}}, Z_{\mathrm{h}})$ for the gear generation process. The coordinate system S_{h} is the reference coordinate system, the coordinate system S_1 denotes the gear blank coordinate system, and the coordinate system $S_{\mathrm{c}}^{(\mathrm{F})}$ represents the rack cutter coordinate system. The rack cutter translates a distance $r_1\phi_1$ during the gear generation process while the gear blank rotates through an angle ϕ_1, where the axis Z_1 represents the rotation axis of the gear.

The common unit normal vector to the rack cutter surface and the generated gear tooth surface at their common contact point passes through the instantaneous axis of rotation I–I according to the gearing theory [5,6]. Therefore, the following condition can be observed:

$$\frac{X_{\mathrm{c}}^{(\mathrm{F})} - x_{\mathrm{c}}^{(\mathrm{F})}}{n_{\mathrm{c}x}^{(\mathrm{F})}} = \frac{Y_{\mathrm{c}}^{(\mathrm{F})} - y_{\mathrm{c}}^{(\mathrm{F})}}{n_{\mathrm{c}y}^{(\mathrm{F})}} = \frac{Z_{\mathrm{c}}^{(\mathrm{F})} - z_{\mathrm{c}}^{(\mathrm{F})}}{n_{\mathrm{c}z}^{(\mathrm{F})}}, \tag{8}$$

where $X_{\mathrm{c}}^{(\mathrm{F})}$, $Y_{\mathrm{c}}^{(\mathrm{F})}$ and $Z_{\mathrm{c}}^{(\mathrm{F})}$ are the coordinates of a point on the instantaneous axis of rotation expressed in coordinate system $S_{\mathrm{c}}^{(\mathrm{F})}$; $x_{\mathrm{c}}^{(\mathrm{F})}$, $y_{\mathrm{c}}^{(\mathrm{F})}$ and $z_{\mathrm{c}}^{(\mathrm{F})}$ denote the coordinates of the instantaneous contact point on the rack cutter surface as expressed by coordinate system $S_{\mathrm{c}}^{(\mathrm{F})}$; symbols $n_{\mathrm{c}x}^{(\mathrm{F})}$, $n_{\mathrm{c}y}^{(\mathrm{F})}$ and $n_{\mathrm{c}z}^{(\mathrm{F})}$ symbolize the components of the common unit normal represented in coordinate system $S_{\mathrm{c}}^{(\mathrm{F})}$. Eq. (8) is termed as meshing equation of the gearing theory. Substituting Eqs. (3) and (7) into Eq. (8) produces the following meshing equation for the rack cutter surface Σ_{F} and gear tooth surfaces:

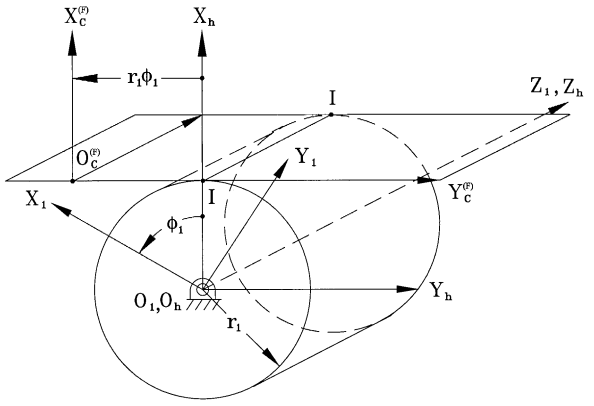

Fig. 5. Relations between coordinate systems $S_{\mathrm{c}}^{(i)}$, S_1 and S_{h}.

$$f(l_F, \theta_F, \phi_1) = \pm \left[l_F - a_F(\cos\psi_n^{(F)} + \tan\psi_n^{(F)} \sin\psi_n^{(F)}) + b_F \sin\psi_n^{(F)} \right] \cos\theta_F + (R_F(1 - \cos\theta_F) - r_1\phi_1) \sin\psi_n^{(F)} = 0. \quad (9)$$

The upper sign in Eq. (9) denotes the meshing equation for the right-side of the rack cutter surface Σ_{FR} and the left-side of the gear tooth surface Σ_{1L}, while the lower sign depicts the meshing equation for the left-side of the rack cutter surface Σ_{FL} and the right-side of the gear tooth surface Σ_{1R}.

2.4. Gear tooth surfaces

The locus of the rack cutter surface Σ_F, expressed in coordinate system S_1, can be obtained by applying the following homogeneous coordinate transformation matrix equation:

$$\mathbf{R}_1^{(F)} = [M_{1c}]\mathbf{R}_c^{(F)}, \quad (10)$$

where

$$[M_{1c}] = \begin{bmatrix} \cos\phi_1 & -\sin\phi_1 & 0 & r_1(\cos\phi_1 + \phi_1 \sin\phi_1) \\ \sin\phi_1 & \cos\phi_1 & 0 & r_1(\sin\phi_1 - \phi_1 \cos\phi_1) \\ 0 & 0 & 1 & 0 \\ 0 & 0 & 0 & 1 \end{bmatrix}$$

and symbol r_1 denotes the radius of the gear pitch circle and ϕ_1 represents the gear rotation angle when the gear is generated by rack cutter Σ_F. The mathematical model of the generated gear tooth surfaces is a combination of the meshing equation and the locus of the rack cutter surfaces according to the gearing theory. Hence, the mathematical model of the gear tooth surfaces can be obtained by simultaneously considering Eqs. (9) and (10). Similarly, the pinion tooth surfaces can be produced by utilizing the same rack cutter that produces the gear tooth surfaces. Therefore, a mathematical model of the pinion tooth surfaces can also be developed by applying the process described above.

3. Computer graphs of the curvilinear-tooth gears

The mathematical model for curvilinear-tooth gears proposed herein can be verified by plotting the gear profile. The coordinates of the curvilinear-tooth gear surface points can be calculated by the developed gear mathematical model and numerical method. A three-dimensional gear tooth profile of the curvilinear-tooth gear can be plotted by the computer graphics.

Table 1 lists some major design parameters of the curvilinear-tooth gears. A three-dimensional gear tooth profile of the curvilinear-tooth gears can be plotted by applying the developed gear mathematical model and computer graphics as depicted in Fig. 6. Fig. 6 reveals that the right- and left-sides of the tooth surfaces of a curvilinear-tooth gear are distinct, and the tooth thickness at the middle section of the tooth flank is larger than at other sections.

Table 1
Design parameters for cylindrical gears with curvilinear shaped teeth

Parameters	Gear	Pinion
Number of teeth	36	18
Normal module (mm)	3	3
Pressure angle (°)	20	20
Face width (mm)	30	30
Nominal radius of the face mill-cutter (mm)	30	30

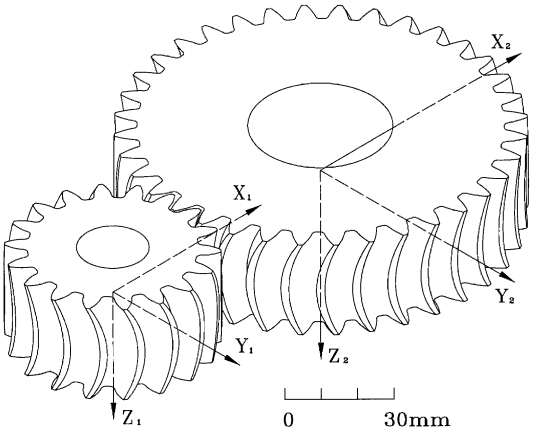

Fig. 6. Cylinderical gears with curvilinear shaped teeth.

4. Tooth undercutting of curvilinear gears

The undercutting of a cylindrical gear with curvilinear shaped teeth can be analyzed by applying the theory of gear singularity proposed by Litvin [6]. According to the concept of differential geometry, a surface point is defined as a singular point if its tangent plane does not exist. The simplest method to check the tooth undercutting of a gear surface is to verify the appearance of singular points on the generated gear tooth surfaces. Let $\mathbf{R}_f^{(F)}$ and $\mathbf{R}_f^{(1)}$ represent the position vectors of tooth surfaces for the rack cutter and generated gear, respectively, as represented in coordinate system $S_f(X_f, Y_f, Z_f)$. The rack cutter surface Σ_F and gear tooth surface Σ_1 have a common contact point at every instant in the generating process. Therefore, the following condition must be observed at their common contact point:

$$\mathbf{R}_f^{(F)} = \mathbf{R}_f^{(1)}. \tag{11}$$

Differentiating Eq. (11) with respect to time yields that

$$\mathbf{V}_{tr}^{(F)} + \mathbf{V}_r^{(F)} = \mathbf{V}_{tr}^{(1)} + \mathbf{V}_r^{(1)}. \tag{12}$$

The subscript "tr" in Eq. (12) denotes the transfer velocity while subscript "r" represents the relative velocity. Thus, Eq. (12) can be rewritten as

$$\mathbf{V}_r^{(1)} = \mathbf{V}_r^{(F)} + \mathbf{V}_{tr}^{(F)} - \mathbf{V}_{tr}^{(1)} = \mathbf{V}_r^{(F)} + \mathbf{V}_{tr}^{(F1)}. \tag{13}$$

The condition for the appearance of a singular point on the tooth surface Σ_1 can be described by equation $\mathbf{V}_{\mathrm{r}}^{(1)} = 0$. Therefore, Eq. (13) becomes

$$\mathbf{V}_{\mathrm{r}}^{(\mathrm{F})} + \mathbf{V}^{(F1)} = 0, \tag{14}$$

where the subscript "tr" in Eq. (14) is omitted for simplicity. Differentiating Eq. (9), the meshing equation for the rack cutter and gear tooth surfaces with respect to time yields

$$\frac{\mathrm{d}}{\mathrm{d}t} f(l_{\mathrm{F}}, \theta_{\mathrm{F}}, \phi_1) = 0. \tag{15}$$

Eqs. (14) and (15) can be rewritten as

$$\frac{\partial \mathbf{R}_{\mathrm{c}}^{(\mathrm{F})}}{\partial l_{\mathrm{F}}} \frac{\mathrm{d}l_{\mathrm{F}}}{\mathrm{d}t} + \frac{\partial \mathbf{R}_{\mathrm{c}}^{(\mathrm{F})}}{\partial \theta_{\mathrm{F}}} \frac{\mathrm{d}\theta_{\mathrm{F}}}{\mathrm{d}t} = -\mathbf{V}_{\mathrm{c}}^{(F1)} \tag{16}$$

and

$$\frac{\partial f}{\partial l_{\mathrm{F}}} \frac{\mathrm{d}l_{\mathrm{F}}}{\mathrm{d}t} + \frac{\partial f}{\partial \theta_{\mathrm{F}}} \frac{\mathrm{d}\theta_{\mathrm{F}}}{\mathrm{d}t} = -\frac{\partial f}{\partial \phi_1} \frac{\mathrm{d}\phi_1}{\mathrm{d}t}, \tag{17}$$

where $\mathbf{R}_{\mathrm{c}}^{(\mathrm{F})}$ depicts the position vector of the rack cutter surface represented in coordinate system S_{c}, and $\mathbf{V}_{\mathrm{c}}^{(\mathrm{F1})}$ denotes the relative velocity of the rack cutter surface Σ_{F} with respect to the gear tooth surface Σ_1 at the instantaneous common contact point represented in coordinate system S_{c}.

Eqs. (16) and (17) determine the limited line L on rack cutter surface Σ_{F} that generates singular points of the gear tooth surface Σ_1. The generating rack cutter surface must be limited to the line L to avert tooth undercutting of the generated gear tooth surface. Eqs. (16) and (17) can be represented by matrix form as

$$\begin{bmatrix} \frac{\partial x_{\mathrm{c}}^{(\mathrm{F})}}{\partial l_{\mathrm{F}}} & \frac{\partial x_{\mathrm{c}}^{(\mathrm{F})}}{\partial \theta_{\mathrm{F}}} \\ \frac{\partial y_{\mathrm{c}}^{(\mathrm{F})}}{\partial l_{\mathrm{F}}} & \frac{\partial y_{\mathrm{c}}^{(\mathrm{F})}}{\partial \theta_{\mathrm{F}}} \\ \frac{\partial z_{\mathrm{c}}^{(\mathrm{F})}}{\partial l_{\mathrm{F}}} & \frac{\partial z_{\mathrm{c}}^{(\mathrm{F})}}{\partial \theta_{\mathrm{F}}} \\ \frac{\partial f}{\partial l_{\mathrm{F}}} & \frac{\partial f}{\partial \theta_{\mathrm{F}}} \end{bmatrix} \begin{bmatrix} \frac{\mathrm{d}l_{\mathrm{F}}}{\mathrm{d}t} \\ \frac{\mathrm{d}\theta_{\mathrm{F}}}{\mathrm{d}t} \end{bmatrix} = \begin{bmatrix} -V_{x\mathrm{c}}^{(F1)} \\ -V_{y\mathrm{c}}^{(F1)} \\ -V_{z\mathrm{c}}^{(F1)} \\ -\frac{\partial f}{\partial \phi_1} \frac{\mathrm{d}\phi_1}{\mathrm{d}t} \end{bmatrix}. \tag{18}$$

Eq. (18) yields a system of four equations in two unknowns: $\mathrm{d}l_{\mathrm{F}}/\mathrm{d}t$ and $\mathrm{d}\theta_{\mathrm{F}}/\mathrm{d}t$. Linear algebra confirms that Eq. (18) has a unique solution when the rank of the augmented matrix is two. This yields

$$\Delta_1 = \begin{vmatrix} \frac{\partial x_{\mathrm{c}}^{(\mathrm{F})}}{\partial l_{\mathrm{F}}} & \frac{\partial x_{\mathrm{c}}^{(\mathrm{F})}}{\partial \theta_{\mathrm{F}}} & -V_{x\mathrm{c}}^{(F1)} \\ \frac{\partial y_{\mathrm{c}}^{(\mathrm{F})}}{\partial l_{\mathrm{F}}} & \frac{\partial y_{\mathrm{c}}^{(\mathrm{F})}}{\partial \theta_{\mathrm{F}}} & -V_{y\mathrm{c}}^{(F1)} \\ \frac{\partial f}{\partial l_{\mathrm{F}}} & \frac{\partial f}{\partial \theta_{\mathrm{F}}} & -\frac{\partial f}{\partial \phi_1} \frac{\mathrm{d}\phi_1}{\mathrm{d}t} \end{vmatrix} = 0, \tag{19}$$

$$\Delta_2 = \begin{vmatrix} \frac{\partial x_{\mathrm{c}}^{(\mathrm{F})}}{\partial l_{\mathrm{F}}} & \frac{\partial x_{\mathrm{c}}^{(\mathrm{F})}}{\partial \theta_{\mathrm{F}}} & -V_{x\mathrm{c}}^{(F1)} \\ \frac{\partial z_{\mathrm{c}}^{(\mathrm{F})}}{\partial l_{\mathrm{F}}} & \frac{\partial z_{\mathrm{c}}^{(\mathrm{F})}}{\partial \theta_{\mathrm{F}}} & -V_{z\mathrm{c}}^{(F1)} \\ \frac{\partial f}{\partial l_{\mathrm{F}}} & \frac{\partial f}{\partial \theta_{\mathrm{F}}} & -\frac{\partial f}{\partial \phi_1} \frac{\mathrm{d}\phi_1}{\mathrm{d}t} \end{vmatrix} = 0, \tag{20}$$

$$\Delta_3 = \begin{vmatrix} \frac{\partial y_c^{(F)}}{\partial l_F} & \frac{\partial y_c^{(F)}}{\partial \theta_F} & -V_{yc}^{(F1)} \\ \frac{\partial z_c^{(F)}}{\partial l_F} & \frac{\partial z_c^{(F)}}{\partial \theta_F} & -V_{zc}^{(F1)} \\ \frac{\partial f}{\partial l_F} & \frac{\partial f}{\partial \theta_F} & -\frac{\partial f}{\partial \phi_1}\frac{d\phi_1}{dt} \end{vmatrix} = 0 \tag{21}$$

and

$$\Delta_4 = \begin{vmatrix} \frac{\partial x_c^{(F)}}{\partial l_F} & \frac{\partial x_c^{(F)}}{\partial \theta_F} & -V_{xc}^{(F1)} \\ \frac{\partial y_c^{(F)}}{\partial l_F} & \frac{\partial y_c^{(F)}}{\partial \theta_F} & -V_{yc}^{(F1)} \\ \frac{\partial z_c^{(F)}}{\partial l_F} & \frac{\partial z_c^{(F)}}{\partial \theta_F} & -V_{zc}^{(F1)} \end{vmatrix} = 0, \tag{22}$$

where Eq. (22) is the same as the meshing equation. Eqs. (19)–(22), if considered simultaneously, can be rewritten as a system of two independent equations with three parameters, l_F, θ_F and ϕ_1 as

$$F(l_F, \theta_F, \phi_1) = \Delta_1^2 + \Delta_2^2 + \Delta_3^2 = 0 \tag{23}$$

and

$$f(l_F, \theta_F, \phi_1) = 0. \tag{24}$$

Since Eqs. (23) and (24) form a system of two independent equations with three unknowns, one of these unknowns, e.g., θ_F, may be selected as an input variable to solve two independent equations with two unknowns l_F and ϕ_1. This system of equations can solve the limited line L on the rack cutter surface that generates the singular points on the generated tooth surface.

The example in Table 2 illustrates the singular points (line of undercutting) on the left- and right-side gear tooth surfaces of the curvilinear-tooth gear. Table 2 illustrates the relationship among the Z_1 component of the gear tooth cross-section and the surface coordinates l_{FL} and l_{FR} under design parameters, $\psi_n^{(F)}$ and R_F, when the singular point appears. l_{FL} represents the surface coordinate of the left-side tooth surface Σ_{1L}, while l_{FR} depicts the surface coordinate of the right-side tooth surface Σ_{1R}. Parameter $\psi_n^{(F)}$ is the normal pressure angle of the gear while R_F is the radius of curve $\widehat{AB}$ (i.e. the nominal radius of the face mill-cutter as depicted in Fig. 1). Table 2 demonstrates that the location of singular points on the middle section of tooth surface Σ_1 is equal to 0.204 mm when the pressure angle of the curvilinear-tooth gear is 20°. The range of rack cutter design parameters l_F is 0.0 mm $\leqslant l_F \leqslant$ 5.652 mm, where $l_F = 0.0$ mm generates the starting point of the involute curve on the tooth surface and $l_F = 5.652$ mm generates the end point of the involute curve (i.e. the tip of addendum). The tooth undercutting occurs on the gear surface when the location of singular points, defined by l_F, ranges from 0.0 to 5.652 mm. The singular points on tooth surfaces are also symmetrical because both sides of the tooth surfaces for the tooth flank of curvilinear-tooth gears are symmetrical. Fig. 7 displays the undercutting line on the tooth surfaces. The tooth undercutting appears near the middle section of the tooth flank when there are 16 teeth as illustrated in Fig. 7(a). The tooth undercutting line covers the whole tooth surface when there are 14 teeth as displayed in Fig. 7(b).

The tooth undercutting phenomenon becomes more severe near the middle section of the tooth flank according to the analysis results depicted in Table 2. According to Fig. 4, the profile of rack cutter on the $X_a^{(F)}$–$Y_a^{(F)}$ plane can be considered as the normal section of rack cutter with helix

Table 2
Location of singular points under different design parameters when module $M_n = 3$ mm and number of teeth = 16 (unit: mm)

Sections	Parameters					
	$\psi_n^{(F)} = 20°$ $R_F = 30$ mm		$\psi_n^{(F)} = 20°$ $R_F = 750$ mm		$\psi_n^{(F)} = 25°$ $R_F = 30$ mm	
Singular points: Z_1	l_{FL}	l_{FR}	l_{FL}	l_{FR}	l_{FL}	l_{FR}
−12.0	−0.308	−0.264	0.204	0.204	−2.077	−2.198
−10.0	−0.135	−0.104	0.204	0.204	−1.862	−1.927
−8.0	−0.005	0.014	0.204	0.204	−1.695	−1.729
−6.0	0.089	0.101	0.204	0.204	−1.571	−1.588
−4.0	0.154	0.159	0.204	0.204	−1.486	−1.492
−2.0	0.192	0.193	0.204	0.204	−1.436	−1.437
0.0	0.204	0.204	0.204	0.204	−1.419	−1.419
2.0	0.192	0.193	0.204	0.204	−1.436	−1.437
4.0	0.154	0.159	0.204	0.204	−1.486	−1.492
6.0	0.089	0.101	0.204	0.204	−1.571	−1.588
8.0	−0.005	0.014	0.204	0.204	−1.695	−1.729
10.0	−0.135	−0.104	0.204	0.204	−1.862	−1.927
12.0	−0.308	−0.264	0.204	0.204	−2.077	−2.198

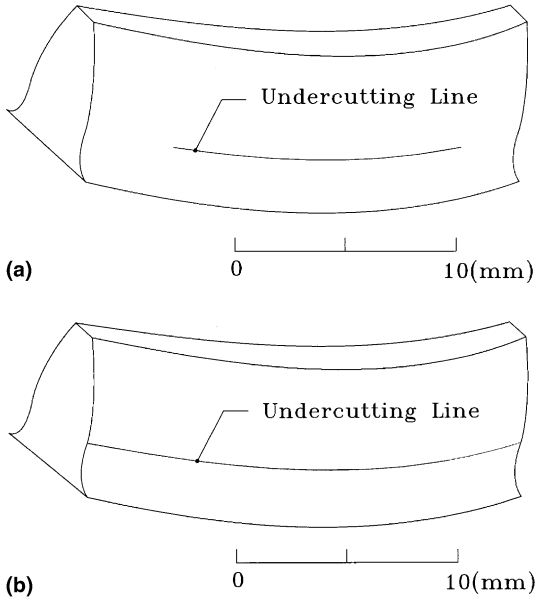

Fig. 7. Undercutting line on tooth surface when the number of teeth is 16 (a) and 14 (b).

angle θ_F. Therefore, the curvilinear-tooth gear generated by this rack cutter can be viewed as an involute gear with varying helical angle across the whole face width, and the pressure angle on the transverse plane can be obtained by

$$\alpha_t = \tan^{-1}\left(\frac{\tan\alpha_n}{\cos\theta_F}\right). \tag{25}$$

According to the fundamentals of involute gearing, the tooth undercutting is occurred easier with a small pressure angle. Therefore, the tooth undercutting phenomenon becomes severer on the transverse planes near the middle of the tooth flank, which have smaller pressure angles.

Singular points, expressed by l_{FL} and l_{FR}, do not have the same location on the right- and left-side tooth surfaces since the right- and left-side tooth surfaces of a curvilinear-tooth gear are different. However, the locations of singular points on the right- and left-side surfaces are more similar closer to the middle section of the tooth flank. In addition, the pressure angle plays an important role in gear tooth undercutting as gears with a smaller pressure angle foster undercutting on tooth surfaces. The profile of a curvilinear-tooth gear approaches that of a spur gear while the nominal radius of face mill-cutter is very large (e.g. $R_F = 750$ mm as illustrated in Table 2). The conditions of tooth undercutting for the right- and left-side tooth surfaces are the same and the conditions of tooth undercutting for each cross-section are also the same when $R_F = 750$ mm. The undercutting characteristics of a curvilinear-tooth gear with $R_F = 750$ mm are almost the same as those of a spur gear. The above results verify that the mathematical models for curvilinear-tooth gear and tooth undercutting proposed herein are correct.

Serious tooth undercutting may reduce the gear strength when the curvilinear-tooth gears have a small number of teeth or pressure angle. The tooth undercutting of curvilinear-tooth gears can be avoided by adopting the profile-shifted generation method. The undercutting analysis reveals that tooth undercutting is significantly easier at the middle section than at other sections of the tooth flank of the curvilinear-tooth gear. Therefore, the tooth undercutting at other sections will not occur if it can be averted at the middle section of the tooth flank. The relationship between the number of teeth and the profile-shifted coefficients for curvilinear-tooth gears is similar to that of the spur gears since the middle section of the curvilinear-tooth gear tooth flank is the same as that of the spur gear.

5. Conclusion

This study has developed a tooth mathematical model of curvilinear-tooth gears having point contacts according to the generation mechanism with a curved-tooth rack cutter. The right- and left-side tooth surfaces of the curvilinear-tooth gears are distinct and the middle section has the largest tooth thickness. It is significantly easier to induce the tooth undercutting phenomena at the middle section of the tooth flank than at other sections. Moreover, although the locations of singular points at the right- and left-side tooth surfaces are not the same, the locations of singular points are more similar closer to the middle section of the tooth flank.

Tooth undercutting of curvilinear-tooth gears can be prevented by employing a positive profile-shifted modification during the gear generation process, and the profile-shifted coefficients for spur gears can also be chosen for the curvilinear-tooth gears when modified curvilinear-tooth gears are generated. The developed tooth mathematical model enables investigations on transmission errors and contact ellipses of the gear set.

Acknowledgements

The authors are grateful to the National Science Council of the Republic of China for the grant. Part of this work was performed under contract No. NSC 89-2212-E-009-013.

References

[1] S.T. Liu, Gear Technology (May/June) (1988) 8–12.
[2] Y. Dai, Y. Ariga, S. Nagata, Tenth World Congress on The Theory of Machine and Mechanisms 6 (1999) 2337–2342.
[3] V. Kin, Gear Technology (November/December) (1990) 30–35.
[4] Z.H. Fong, C.B. Tsay, ASME Journal of Mechanical Design 114 (2) (1992) 317–325.
[5] F.L. Litvin, Theory of Gearing, NASA Reference Publication 1212, Washington, DC, 1989.
[6] F.L. Litvin, Gear Geometry and Applied Theory, Prentice-Hall, Englewood Cliffs, NJ, 1994.